Effect of attractive interaction on instability of pedestrian flow in a two-dimensional optimal velocity model

Akihiro Nakayama*
Department of Physics, Meijo University, Nagoya, 468-8502, Japan

Katsuya Hasebe†
Faculty of Business Administration, Aichi University, Miyoshi, Aichi 470-0296, Japan

Yūki Sugiyama‡
Department of Complex Systems Science, Nagoya University, Nagoya 464-8601, Japan

(Received 25 August 2007; revised manuscript received 22 October 2007; published 14 January 2008)

We incorporate an attractive interaction in a two-dimensional optimal velocity model and investigate the stability of homogeneous flow in the linear approximation. There exists a different type of instability in this model. We show the phase diagram and the behavior of the flow in each phase by numerical simulations. A new phase due to the new instability appears at low density, and the instability can be a candidate of the group formation mechanism of organisms.

DOI: 10.1103/PhysRevE.77.016105 PACS number(s): 89.40.−a, 45.70.Vn, 05.70.Fh, 07.05.Tp

I. INTRODUCTION

Traffic flow, pedestrian flow, and some related systems present interesting phenomena and have been studied from the physical viewpoint [1–5]. Pedestrian flow is an important issue also from the engineering viewpoint [6,7] and various models have been proposed to explain the dynamical behavior of pedestrians and to apply to realistic problems [8–16]. In a previous paper, we proposed a two-dimensional optimal velocity (OV) model to study the pedestrian dynamics [17]. In the model the motion of pedestrians is described by a simple dynamical equation of motion and we can investigate the property of pedestrian flow not only numerically but also analytically. In the work, we supposed that the interaction among pedestrians is repulsive because pedestrians keep a certain distance from others to avoid collisions. We obtained the stability condition of homogeneous flow of pedestrians and also clarified the phase structure in this model.

As a system related to pedestrians, the collective motion of various organisms has interesting features and has been investigated [18–29]. In such models, the interactions among organisms are supposed to be repulsive (separation effect) at a short distance and attractive (cohesion effect) at a large distance. The separation force is quite similar to the interaction among pedestrians, and the existence of attractive force is one of the differences between pedestrians and organisms. Thus it is an interesting problem how the attractive interaction changes the property of pedestrian flow.

In this paper, we introduce the attractive interaction to the two-dimensional OV model and investigate the effect of the attractive interaction to the instability of pedestrian flow. The interaction in the model is expressed by a single function (OV function), and we can introduce the attractive interaction only by changing a parameter of the OV function. By restricting the interaction as above, we can understand both one- and two-dimensional phenomena in a unified way [33]. First we estimate the stability conditions of the homogeneous flow solution in the linear approximation. From these results, we can draw the phase diagrams. The behavior of the flow in each phase is confirmed by numerical simulations.

In Sec. II we present a brief review of the two-dimensional OV model. We carry out the linear analysis of the homogeneous flow and find the stability conditions in Sec. III. The property of the stability condition is investigated in Sec. IV. In Sec. V, we show the phase diagrams and the snapshots of the flow in some typical cases. Section VI is devoted to summary and discussion.

II. TWO-DIMENSIONAL OV MODEL

First we briefly review the two-dimensional OV model [17]. In the model, pedestrians are treated as identical point particles moving in the two-dimensional space. The basic concept of the OV model is that each particle controls its acceleration in order to reduce the difference between the optimal velocity and its real velocity. The optimal velocity is decided by its "desired velocity" and interactions with other particles. A particle moves with the desired velocity, if it is alone. The model is expressed by the equation of motion

$$\frac{d^2}{dt^2}\vec{x}_j(t) = a\left[\{\vec{V}_0 + \sum_k \vec{F}[\vec{r}_{kj}(t)]\} - \frac{d}{dt}\vec{x}_j(t)\right], \tag{1}$$

$$\vec{F}(\vec{r}_{kj}) = f(r_{kj})(1+\cos\theta)\vec{n}_{kj}, \tag{2}$$

$$f(r_{kj}) = \alpha[\tanh\beta(r_{kj}-b)+c], \tag{3}$$

where $\vec{x}_j=(x_j,y_j)$ is the position of the jth particle, and $\vec{r}_{kj}=\vec{x}_k-\vec{x}_j$, $r_{kj}=|\vec{r}_{kj}|$, $\cos\theta=(x_k-x_j)/r_{kj}$, and $\vec{n}_{kj}=\vec{r}_{kj}/r_{kj}$. a is "sensitivity," which represents the strength of reaction of

*spock@ccmfs.meijo-u.ac.jp
†hasebe@vega.aichi-u.ac.jp
‡sugiyama@phys.cs.is.nagoya-u.ac.jp

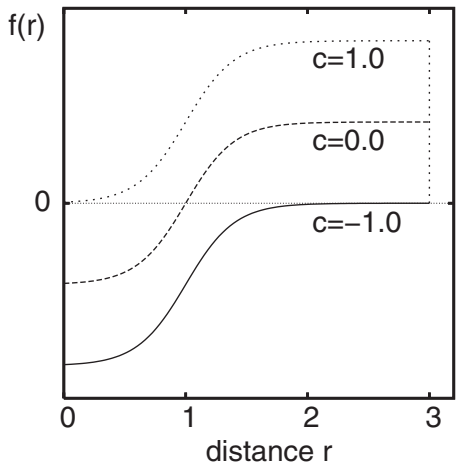

FIG. 1. r-dependence of the interaction. The interaction is attractive for $f(r)>0$ and repulsive for $f(r)<0$. Solid, dashed, and dotted lines represent $f(r)$ for the cases $c=-1$, $c=0$, and $c=1$, respectively. The vertical line at $r=3$ represents the cutoff of $f(r)$. In numerical simulations the value of cutoff is varied depending on the density of particles.

each particle. For simplicity, particles are supposed to move in the positive direction of the x axis, and $\vec{V}_0=(V_0,0)$ is a constant vector which expresses the desired velocity. $\vec{F}=(F_x,F_y)$ expresses the interaction between particles and its form is a straightforward extension of the one-dimensional OV model. In order that $\vec{F}$ has the same dimension as $\vec{V}$, parameters α,β,b are supposed to have suitable dimensions. Due to the factor $(1+\cos\theta)$, a particle is more sensitive to particles in front than those behind. By taking this form, we can understand both one- and two-dimensional phenomena in a unified way.

In numerical simulations and in the estimation of explicit values, we set $\alpha=1/4$, $\beta=2.5$, and $b=1$, for convenience. The sole role of $\vec{V}_0$ is to fix the direction of motion and the magnitude V_0 is meaningless, because V_0 can be changed arbitrarily by the coordinate transformation. The parameter c is varied in the range $-1\leq c\leq 1$ (see Fig. 1). $c=-1$ means that the interaction is repulsive, and $c=1$ means that the interaction is attractive. For the other c, the interaction is attractive at large distance and repulsive at short distance.

Here we note that the cutoff of the attractive interaction is necessary to avoid the divergence of the summation over all particles. In the linear analysis it is satisfied by considering only the nearest-neighbor interaction, and in numerical simulations we introduce the cutoff at an appropriate value which can take into account the nearest-neighbor interaction.

Next we derive the linearized equation in the same way as the previous paper [17]. In Eq. (1), there is a homogeneous flow solution

$$(x_j,y_j)=(X_j+v_xt,Y_j+v_yt), \tag{4}$$

where (X_j,Y_j) represents sites on a triangular lattice as shown in the Appendix. All particles move at a constant velocity

$$v_x=V_0+\sum_k F_x(X_k-X_j,Y_k-Y_j),$$

$$v_y=\sum_k F_y(X_k-X_j,Y_k-Y_j). \tag{5}$$

From now on we consider only the nearest-neighbor interaction, and the summation of Eq. (5) is taken over six particles. By considering a small perturbation on the homogeneous flow solution (4), we obtain the linearized equation

$$\frac{d^2}{dt^2}x_j=\sum_k\left[A_k(x_k-x_j)+B_k(y_k-y_j)\right]-\frac{d}{dt}x_j,$$

$$\frac{d^2}{dt^2}y_j=\sum_k\left[C_k(x_k-x_j)+D_k(y_k-y_j)\right]-\frac{d}{dt}y_j, \tag{6}$$

where

$$A_k=\partial_xF_x(x,y)|_{x=X_k-X_j,y=Y_k-Y_j},$$

$$B_k=\partial_yF_x(x,y)|_{x=X_k-X_j,y=Y_k-Y_j},$$

$$C_k=\partial_yF_y(x,y)|_{x=X_k-X_j,y=Y_k-Y_j},$$

$$D_k=\partial_yF_y(x,y)|_{x=X_k-X_j,y=Y_k-Y_j}. \tag{7}$$

For simplicity, we removed the sensitivity a by the replacement $t\to t/a$, $V_0\to aV_0$, $F\to aF$. We can easily restore a in the final result by the inverse replacement. The explicit forms of A_k, B_k, C_k, and D_k are shown in the Appendix.

III. STABILITY CONDITION

In this section we discuss mode solutions of the linearized Eq. (6) and their stability conditions. In previous works we have considered the mode solutions whose polarizations are fixed. Here a different formulation is adopted to find a different condition.

Generally, the mode solutions can be written as

$$x_j=\epsilon_1\exp[i\omega t+i(kX_j+mY_j)], \tag{8}$$

$$y_j=\epsilon_2\exp[i\omega t+i(kX_j+mY_j)], \tag{9}$$

where the wave vector (k,m) is a constant vector but the polarization (ϵ_1,ϵ_2) is not supposed to be a constant. Then the linearized equations become

$$-\epsilon_1\omega^2=\epsilon_1\bar{A}+\epsilon_2\bar{B}-i\epsilon_1\omega, \tag{10}$$

$$-\epsilon_2\omega^2=\epsilon_1\bar{C}+\epsilon_2\bar{D}-i\epsilon_2\omega, \tag{11}$$

where

$$\bar{A}=2\{(A_1+A_5)(\cos ks\cos mu-1)+A_3(\cos 2mu-1)\}+2i(A_1-A_5)\sin ks\cos mu, \tag{12}$$

$$\bar{D}=2\{(D_1+D_5)(\cos ks\cos mu-1)+D_3(\cos 2mu-1)\}+2i(D_1-D_5)\sin ks\cos mu, \tag{13}$$

$$\bar{B} = -2(B_1 - B_5)\sin ks \sin mu + 2i(B_1 + B_5)\cos ks \sin mu, \tag{14}$$

$$\bar{C} = -2(C_1 - C_5)\sin ks \sin mu + 2i\{(C_1 + C_5)\cos ks \sin mu + C_3 \sin 2mu\}. \tag{15}$$

Here $s = r\cos(\pi/6)$ and $u = r\sin(\pi/6)$ and r is the distance among particles (see the Appendix).

The stability condition of the homogeneous flow is given by the condition that all of $\omega(k,m)$ does not have the negative imaginary part. The analysis is divided to three parts depending on the polarization (ϵ_1, ϵ_2) for convenience.

(1) $(\epsilon_1, \epsilon_2) = (\epsilon, 0)$.

In this case the polarization is fixed, and the analysis is reduced to that in the previous paper. Here we show the results in two typical cases.

(a) $m = 0$: longitudinal mode along the x-axis.

(b) $k = 0$: transverse mode along the y-axis.

(2) $(\epsilon_1, \epsilon_2) = (0, \epsilon)$.

In the same way as above, we show the results in two cases.

(a) $m = 0$: transverse mode along the x-axis.

(b) $k = 0$: longitudinal mode along the y-axis.

(3) $(\epsilon_1, \epsilon_2) = (1, \epsilon)$.

This is a different type of mode solutions and is polarized elliptically. The polarization is not constant but depends on the particle distance r. The results in this case include those in (1a), (1b), (2a), and (2b) as special cases.

A. Longitudinal mode along the x axis

Substituting $(\epsilon_1, \epsilon_2) = (\epsilon, 0)$ and $m = 0$ into Eqs. (10) and (11), we find

$$-\omega^2 = \bar{A} - i\omega, \tag{16}$$

$$\bar{C} = 0, \tag{17}$$

where

$$\bar{A} = 2(A_1 + A_5)(\cos ks - 1) + 2i(A_1 - A_5)\sin ks. \tag{18}$$

The constraint (17) is trivially satisfied and the stability condition is given by

$$a > 4\frac{(A_1 - A_5)^2}{A_1 + A_5}, \tag{19}$$

where we restored the sensitivity a by the replacement $F \to F/a$. From Eq. (19), we can find critical curves, which are the border of the stable region, and show them in typical cases (see Fig. 2).

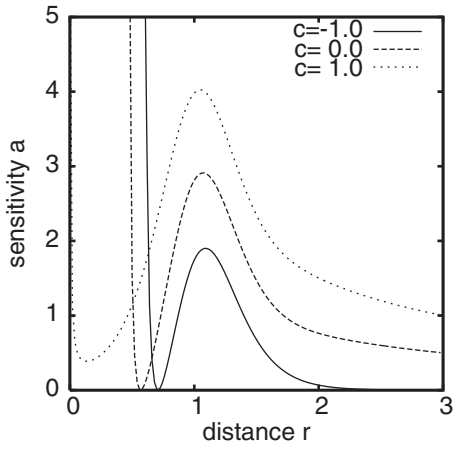

FIG. 2. Solid, dashed, and dotted curves represent the critical curves given by Eq. (19) for the cases $c=-1$, $c=0$, and $c=1$, respectively. The homogeneous flow is stable in the region above each curve.

B. Transverse mode along the y axis

In this case $(\epsilon_1, \epsilon_2) = (\epsilon, 0)$ and $k = 0$. Then Eqs. (10) and (11) become

$$-\omega^2 = \bar{A} - i\omega, \tag{20}$$

$$\bar{C} = 2i \sin mu\{(C_1 + C_5) + 2C_3 \cos mu\} = 0, \tag{21}$$

where $\bar{A} = 2\{(A_1 + A_5)(\cos mu - 1) + A_3(\cos 2mu - 1)\}$. Because $\bar{A}$ is real, the stability condition is $\bar{A} < 0$.

There are two solutions of the constraint (21).

(i) $\sin mu = 0$.

The unstable mode exists for $mu = \pi$ only because $(k,m) = (0,0)$ is a stable mode. Then the stability condition is

$$A_1 + A_5 > 0. \tag{22}$$

(ii) $(C_1 + C_5) + 2C_3 \cos mu = 0$.

In this case both of following two inequalities are the stability condition:

$$\left| -\frac{C_1 + C_5}{2C_3} \right| \leq 1, \tag{23}$$

$$\bar{A} = \frac{1}{C_3}\{2C_3(A_1 + 2A_3 + A_5) + (A_1 + A_5)(C_1 + C_5) - (C_1 + C_5)^2\} < 0. \tag{24}$$

Table I shows the numerical values of Eqs. (22)–(24) in typical cases. These values are calculated in the cases of α

TABLE I. Solutions of the conditions (22)–(24) in the cases of $c=-1.0$, -0.5, 0.0, 0.5, and 1.0.

	$c=-1.0$	$c=-0.5$	$c=0.0$	$c=0.5$	$c=1.0$
(i)	$r>0.59$	$r>0.54$	$r>0.47$	$r>0.36$	$r>0.0$
(ii)	$r>0.94$	$r>0.84$	$r>0.73$	$r>0.58$	$r>0.0$

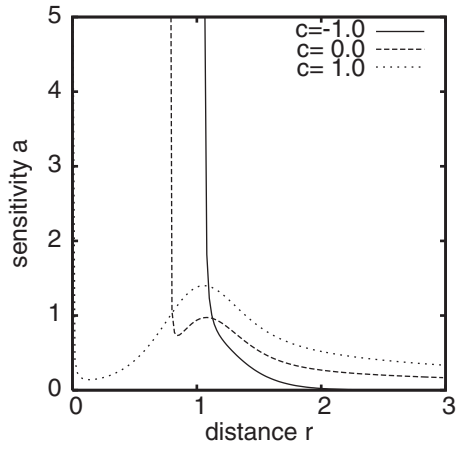

FIG. 3. Solid, dashed, and dotted curves represent the critical curves given by Eq. (28) for the cases $c=-1$, $c=0$, and $c=1$, respectively. The homogeneous flow is stable in the region above each curve.

$=1/4$, $\beta=2.5$, and $b=1$. Hereafter we will calculate critical values in the same parameter.

C. Transverse mode along the x axis

Substituting $(\epsilon_1,\epsilon_2)=(0,\epsilon)$ and $m=0$ into Eqs. (10) and (11), we find

$$\bar{B}=0, \tag{25}$$

$$-\omega^2=\bar{D}-i\omega, \tag{26}$$

where

$$\bar{D}=2(D_1+D_5)(\cos ks-1)+2i(D_1-D_5)\sin ks. \tag{27}$$

The constraint (25) is trivially satisfied and the stability condition is

$$a>4\frac{(D_1-D_5)^2}{D_1+D_5}. \tag{28}$$

Figure 3 shows the plots of Eq. (28) for typical cases.

D. Longitudinal mode along the y axis

In this case $(\epsilon_1,\epsilon_2)=(0,\epsilon)$ and $k=0$. Then Eqs. (10) and (11) are

$$\bar{B}=2i(B_1+B_5)\sin mu=0, \tag{29}$$

$$-\omega^2=\bar{D}-i\omega, \tag{30}$$

where $\bar{D}=2\{(D_1+D_5)(\cos mu-1)+D_3(\cos 2mu-1)\}$. Because $\bar{D}$ is real, the stability condition is $\bar{D}<0$. The constraint (29) indicates $mu=\pi$, and the stability condition becomes

$$D_1+D_5>0. \tag{31}$$

Table II shows the numerical values of Eq. (31) for typical cases.

TABLE II. Solutions of the condition (31) in the cases of $c=-1.0$, -0.5, 0.0, 0.5, and 1.0.

$c=-1.0$	$c=-0.5$	$c=0.0$	$c=0.5$	$c=1.0$
$r>1.05$	$r>0.91$	$r>0.78$	$r>0.62$	$r>0.0$

E. Elliptically polarized mode

After the substitution of $(\epsilon_1,\epsilon_2)=(1,\epsilon)$ into Eqs. (10) and (11), we rewrite the equations as follows:

$$(\bar{B})\epsilon^2+(\bar{A}-\bar{D})\epsilon-\bar{C}=0, \tag{32}$$

$$\omega^2-i\omega+\bar{A}+\epsilon\bar{B}=0. \tag{33}$$

These are second order algebraic equations with respect to ω and ϵ, and we can solve these equations. There are two solutions $\epsilon[k,m,f(r)]$ and four solutions $\omega[k,m,f(r)]$ in general. However, those are too complicated and we cannot obtain the stability condition for k, m, $f(r)$. Instead, we solve Eqs. (32) and (33) for each (k,m) and r numerically. Then we can search the condition that all of ω do not have the negative imaginary part. The results for typical cases are shown in Fig. 4.

For the case $c=0.0$ we find that the critical curve in Fig. 4 consists of three parts: left vertical curve, middle curve, and right vertical line. The left curve is the same as that in Fig. 3, and the middle curve is the same as that in Fig. 2. To see the coincidence of the critical curves, we show the critical curve and Eqs. (19) and (28) in Fig. 5.

This result can be understood as follows. The elliptically polarized mode reduces to (1a),(1b) in the case $\epsilon\to 0$, and reduces to (2a),(2b) in the case $\epsilon\to\infty$. It is natural that the conditions (19) and (28) are included in this mode.

On the other hand, there is no corresponding condition for the vertical line (for example, at $r=1.39$ for $c=0.0$) in other modes. This stability condition appears only in the elliptic

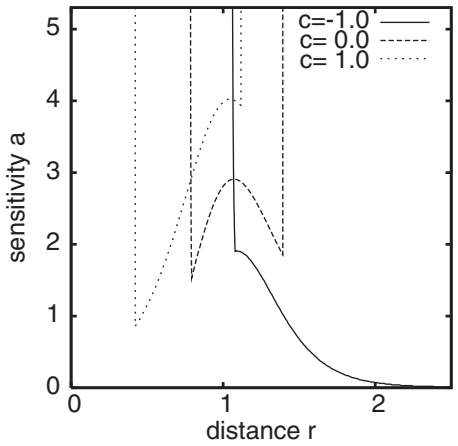

FIG. 4. Solid, dashed, and dotted curves represent the critical curves obtained by solving Eqs. (32) and (33) numerically for the cases $c=-1$, $c=0$, and $c=1$, respectively. The homogeneous flow is stable in the region above each curve. In the cases $c=0$ and $c=1$, the stable region is enclosed by curves.

TABLE III. Numerical values corresponding to the vertical lines in Fig. 4. The values are obtained by solving Eqs. (32) and (33) numerically for the cases of $c=-1.0$, -0.5, 0.0, 0.5, and 1.0.

$c=-1.0$	$c=-0.5$	$c=0.0$	$c=0.5$	$c=1.0$
$r<+\infty$	$r<1.58$	$r<1.39$	$r<1.26$	$r<1.12$

mode. Table III shows the values corresponding to the vertical lines, those are obtained by solving Eqs. (32) and (33) numerically in typical cases.

IV. STABILITY CONDITION

We investigate the stability condition which is obtained by solving the linearized equation numerically in the previous section. Numerical simulations (see Sec. V) indicate that the instability due to elliptically polarized modes starts from long wavelength modes. Then we use the long wavelength approximation $k,m\to 0$.

If we take the first order of k and m, Eqs. (12)–(15) become

$$\bar{A} \sim 2i(A_1 - A_5)ks,$$

$$\bar{D} \sim 2i(D_1 - D_5)ks,$$

$$\bar{B} \sim 2i(B_1 + B_5)mu,$$

$$\bar{C} \sim 2i(C_1 + C_5 + 2C_3)mu, \tag{34}$$

that is, $\bar{A},\bar{B},\bar{C},\bar{D}\ll 1$. The solution of Eq. (32) is

$$\epsilon = \frac{1}{2\bar{B}}\{-(\bar{A}-\bar{D}) \pm \sqrt{(\bar{A}-\bar{D})^2 + 4\bar{B}\bar{C}}\}, \tag{35}$$

and therefore $\bar{A}+\epsilon\bar{B}\ll 1$. By use of this approximation, the solution of Eq. (33) is

$$\omega = \frac{1}{2}\{i \pm \sqrt{-1 - 4(\bar{A}+\epsilon\bar{B})}\} \sim \frac{i}{2}\{1 \pm [1 + 2(\bar{A}+\epsilon\bar{B})]\}$$

$$= i(1 + \bar{A} + \epsilon\bar{B}), \quad -i(\bar{A}+\epsilon\bar{B}). \tag{36}$$

The first solution in Eq. (36) has a positive imaginary part, and unstable modes exist only in the second solution. Substituting Eqs. (34) and (35) into the second solution in Eq. (36), we find

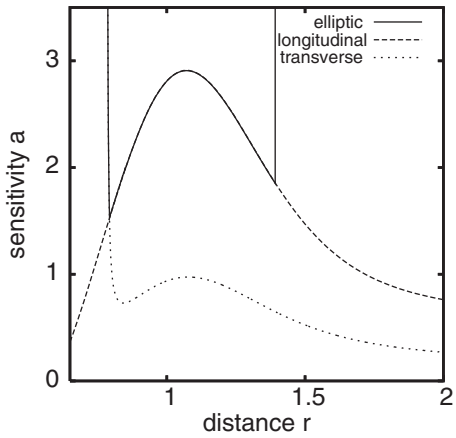

FIG. 5. Critical curves for the case $c=0$. Solid curve is obtained by solving Eqs. (32) and (33) numerically. Dashed and dotted curves represent the critical curves given by Eqs. (19) and (28), respectively.

$$\omega = (A_1 - A_5 + D_1 - D_5)ks \pm [(A_1 - A_5 - D_1 + D_5)^2(ks)^2 + 4(B_1 + B_5)(C_1 + C_5 + 2C_3)(mu)^2]^{1/2}. \tag{37}$$

Only in the case of $(B_1+B_5)(C_1+C_5+2C_3)<0$, ω can have a negative imaginary part for appropriate k,m, for example, $k=0$ and $m>0$. Then the stability condition is

$$(B_1 + B_5)(C_1 + C_5 + 2C_3) > 0. \tag{38}$$

Table IV shows the numerical values of Eq. (38) with the results in Sec. III. The values obtained from Eq. (38) coincide with those in Table III completely. The critical values for Eq. (38) in Table IV can be calculated by $C_1+C_5+2C_3=0$ or $B_1+B_5=0$. By comparison with the critical values for the conditions (23) and (24), we find that the condition originates from $B_1+B_5=0$.

V. NUMERICAL SIMULATION AND PHASE DIAGRAMS

From the stability conditions obtained in Secs. III and IV, we can draw the phase diagrams. Figures 6(a)–6(c) are the phase diagrams for $c=-1.0$, $c=0.0$, and $c=1.0$, respectively. The homogeneous flow is stable in the region S. L represents the region where only longitudinal modes along the x axis (density wave) are unstable. In the region T, only transverse modes along the x axis are unstable, and in the region E, only elliptically polarized modes are unstable.

The behavior of the flow is investigated by numerical simulations. Figures 7–9 show snapshots of the flow ob-

TABLE IV. Solutions of the stability conditions (22) and (23) with Eqs. (24), (38), and (31) in the cases of $c=-1.0$, -0.5, 0.0, 0.5, and 1.0.

	$c=-1.0$	$c=-0.5$	$c=0.0$	$c=0.5$	$c=1.0$
Equation (22)	$0.59<r$	$0.54<r$	$0.47<r$	$0.36<r$	$0.0<r$
Equations (23) and (24)	$0.94<r$	$0.84<r$	$0.73<r$	$0.58<r$	$0.0<r$
Equation (38)	$0.94<r$	$0.84<r<1.58$	$0.73<r<1.39$	$0.58<r<1.26$	$0.42<r<1.12$
Equation (31)	$1.05<r$	$0.91<r$	$0.78<r$	$0.62<r$	$0.0<r$

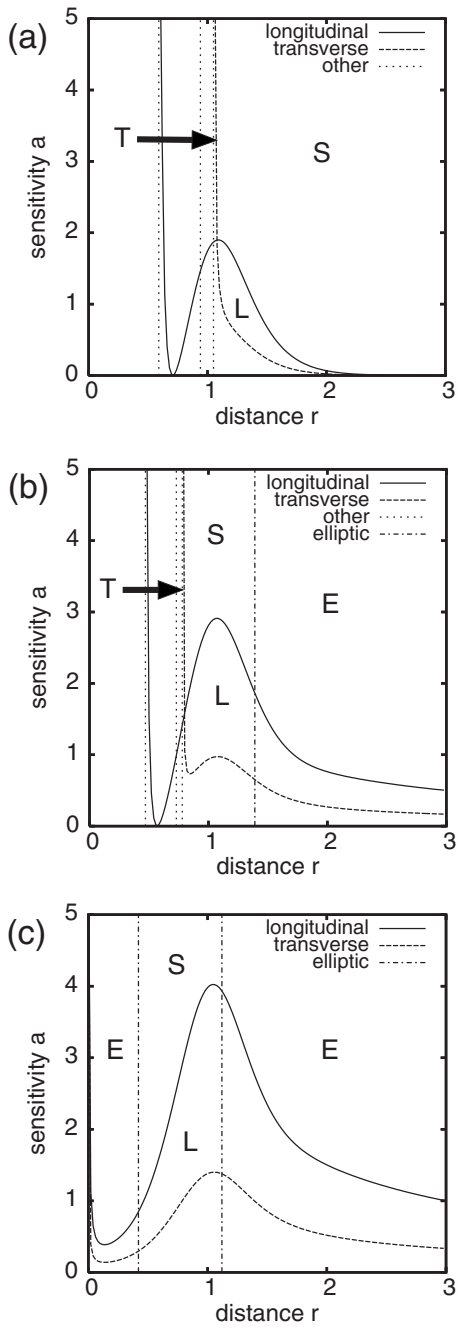

FIG. 6. Phase diagrams for the cases (a) $c=-1.0$, (b) $c=0.0$, and (c) $c=1.0$. Solid and dashed curves are critical curves for longitudinal and transverse modes along the x axis, respectively. Dotted lines are critical lines for modes along the y axis. Dashed dotted lines are critical lines for elliptically polarized modes. S represents the region where the homogeneous flow is stable. L represents the region where only longitudinal modes along the x axis are unstable. In the narrow region T between dashed and dotted lines, only transverse modes along the x axis are unstable, and in the region E only the elliptically polarized modes are unstable.

tained by numerical simulations in the case $c=0.0$ [see Fig. 6(b)]. All simulations are carried out in the periodic boundary conditions along both the x and y axes, and all particles are supposed to move in the positive x direction. In order to compare with the results of the linear analysis, we set the

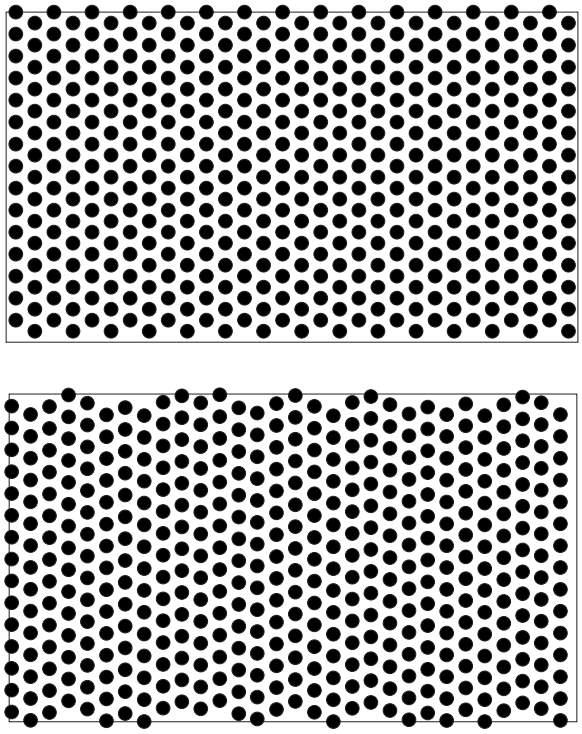

FIG. 7. Snapshots of the flow after a sufficiently large number of simulation steps for the case $c=0.0$. Boundary conditions are periodic along the x and y axes. Parameters in the figure (a) $r=1.0$, $a=5.0$ and (b) $r=0.785$, $a=3.0$ correspond to the region (s) and (t), respectively. We use black disks to show the position of particles clearly. All particles are supposed to move rightward.

homogeneous flow as the initial condition, except for Figs. 9(c) and 9(d). In numerical simulations, the flow in the above four regions can be easily distinguished and the boundaries among them are identified clearly. In other regions where several modes are unstable simultaneously, the behaviors of the flow are complicated and the boundaries among them are not clear.

Figure 7(a) is the snapshot in the case of $r=1.0$ and $a=5.0$. The parameters exist in the region (S) where the homogeneous flow is stable. This snapshot shows the flow after sufficient relaxation time, but it is the same as the initial flow.

Figure 7(b) is the snapshot in the case of $r=0.785$ and $a=3.0$, where transverse modes along the x axis are unstable (T). The snapshot shows the flow after sufficient relaxation time. We can see that the transverse waves have emerged.

Figure 8 is the snapshots in the case of $r=1.0$ and $a=2.0$, where longitudinal modes along the x axis are unstable (L). Figure 8(a) is a snapshot in the early stage and Fig. 8(b) shows the flow after sufficient relaxation time. We can see that some defects emerge but the homogeneity remains in a large part of the flow. The flow is characterized by the emergence of the density wave, and this phase just corresponds to the congested phase of traffic flow.

Figure 9 is the snapshots in the case of $r=2.0$ and $a=3.0$, where elliptically polarized modes are unstable (E). Figure 9(a) shows the flow in the early stage, where the elliptically polarized mode is enhanced. After a sufficiently

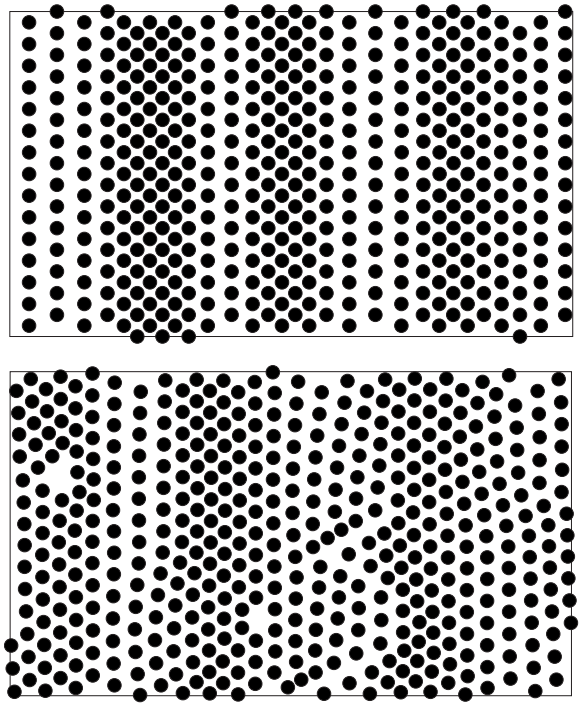

FIG. 8. Snapshots of the flow for the case $c=0.0$, $r=1.0$, and $a=2.0$. The parameters correspond to the region (l). (a) The flow at the early stage and (b) the flow after a sufficiently large number of simulation steps.

large number of simulation steps, particles make several isolated groups and the homogeneity is completely broken [see Fig. 9(b)]. Here we note that this property of making groups is common to the cases of $-1<c\leq 1$ except for the distance among particles in groups, which depend on the value of c.

We consider that the resulting pattern of the flow in the region (E) is characterized by the formation of groups. If we change the initial conditions, different patterns emerge, but they are qualitatively the same. For example, Fig. 9(d) is the result of a simulation in the different initial condition Fig. 9(c) with the same parameters as Figs. 9(a) and 9(b). The difference between Figs. 9(b) and 9(d) is not essential from the physical viewpoint.

VI. SUMMARY AND DISCUSSION

In this paper, we have investigated the stability conditions of the homogeneous flow in the two-dimensional OV model with attractive interaction. We found a stability condition for the elliptically polarized modes. The instability originating from these modes appears only in the model with attractive interaction, and changes the phase structure as shown in Fig. 6. In the completely repulsive case ($c=-1$), the low density flow is stable. If the attractive interaction exists, the low density flow is no longer stable. In this case the stable region exists only around $r\sim 1$. We may naturally expect that the flow is stable at r where the OV function $f(r)$ is zero, that is, no force act among particles. However, the stable region $r\sim 1$ does not correspond to such r, but corresponds to the region where the OV function has a large (positive) gradient. This is a specific feature of the elliptically polarized modes because other modes are unstable in the region. This property depends both on the dynamics and on the form of OV function. We cannot find an intuitive interpretation why the homogeneous flow is stable in such a region.

We find that both of the sparse and dense homogeneous flows are not stable if the attractive interaction exists. In such cases the final state of the flow depends on the detail of the model. In the present model, particles make several stable groups and there is no interaction among groups due to the cutoff of the interaction (see Fig. 8). It is known that pedestrians have a tendency to make groups [10]; but we have no

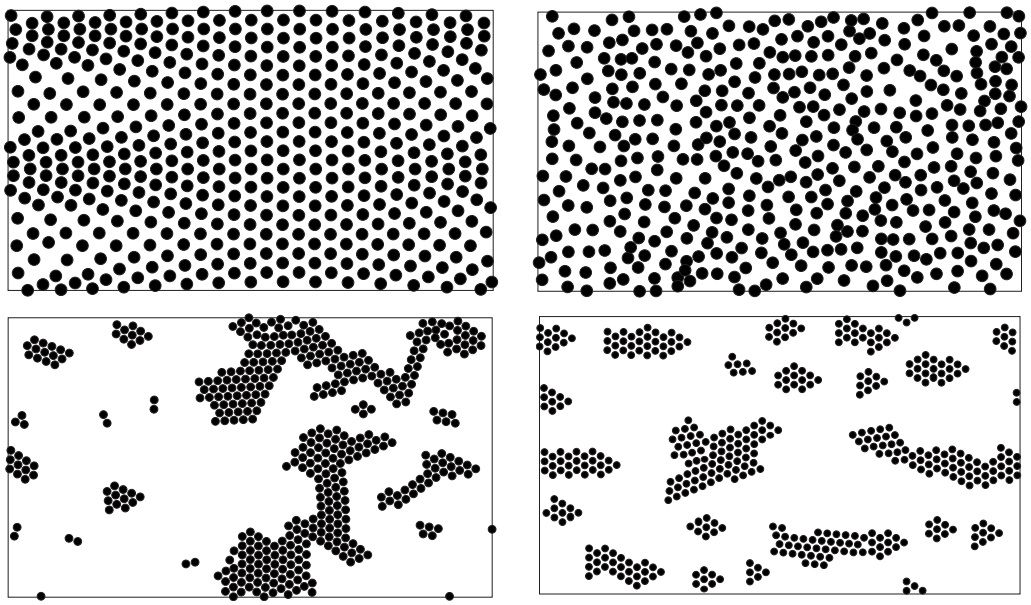

FIG. 9. Snapshots of the flow for the case $c=0.0$, $r=2.0$, and $a=3.0$. The parameters correspond to the region (e). (a) The flow at the early stage and (b) the flow after a sufficiently large number of simulation steps. (c) The initial flow of randomly distributed particles and (d) is its developed state after a sufficiently large number of simulation steps.

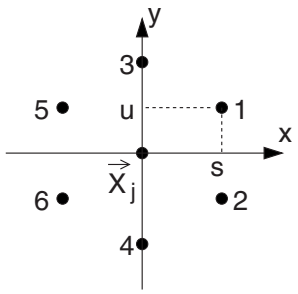

FIG. 10. Positions and indices of nearest neighbor particles are shown. For example, the position of the particle 1 is (s,u), where the distance r is $\sqrt{s^2+u^2}$.

detailed data of the motion of pedestrians to compare with numerical simulations. On the other hand, it is well-known that most organisms often form groups, for example, fish school or flock of birds. We can expect that the instability of sparse homogeneous flow and the resulting formation of groups are general features of such biological systems. This mechanism can be a candidate for the explanation of the group formation of organisms [30–32].

ACKNOWLEDGMENT

This work was partly supported by a Grant-in-Aid for Scientific Research (C) of the Ministry of Education, Science, Sports and Culture of Japan (No. 18540409).

APPENDIX: EXPLICIT FORMS OF *A*, *B*, *C*, *D*

We assign the number to particles around the jth particle as shown in Fig. 10. For example, the position of particle 1 is $(s,u)=(r\cos[\pi/6], r\sin[\pi/6])$, where r is the distance between two nearest-neighbor particles.

Then the parameters $A_1, A_2, \ldots, A_6, B_1, B_2, \ldots, D_6$ [e.g., $A_1=\partial_x F_x(x,y)|_{x=s,y=u}$] are

$$\begin{Bmatrix} A_1 \\ A_5 \end{Bmatrix} = f'\left(\frac{3}{4} \pm \frac{3\sqrt{3}}{8}\right) + \frac{f}{r}\left(\frac{1}{4} \pm \frac{\sqrt{3}}{4}\right), \tag{A1}$$

$$\begin{Bmatrix} B_1 \\ B_5 \end{Bmatrix} = f'\left(\frac{3}{8} \pm \frac{\sqrt{3}}{4}\right) + \frac{f}{r}\left(-\frac{3}{4} \mp \frac{\sqrt{3}}{4}\right), \tag{A2}$$

$$\begin{Bmatrix} C_1 \\ C_5 \end{Bmatrix} = f'\left(\frac{3}{8} \pm \frac{\sqrt{3}}{4}\right) + \frac{f}{r}\left(-\frac{1}{4} \mp \frac{\sqrt{3}}{4}\right), \tag{A3}$$

$$\begin{Bmatrix} D_1 \\ D_5 \end{Bmatrix} = f'\left(\frac{1}{4} \pm \frac{\sqrt{3}}{8}\right) + \frac{f}{r}\left(\frac{3}{4} \pm \frac{\sqrt{3}}{4}\right), \tag{A4}$$

$$A_3 = C_3 = \frac{f}{r}, \quad D_3 = f', \tag{A5}$$

and

$$A_1 = A_2, \quad A_3 = A_4, \quad A_5 = A_6,$$

$$B_1 = -B_2, \quad B_3 = -B_4 = 0, \quad B_5 = -B_6,$$

$$C_1 = -C_2, \quad C_3 = -C_4, \quad C_5 = -C_6,$$

$$D_1 = D_2, \quad D_3 = D_4, \quad D_5 = D_6. \tag{A6}$$

[1] *Workshop on Traffic and Granular Flow*, edited by D. E. Wolf, M. Schreckenberg, and A. Bachem (World Scientific, Singapore, 1996).

[2] *Workshop on Traffic and Granular Flow '97*, edited by M. Schreckenberg and D. E. Wolf (Springer-Verlag, Singapore, 1998).

[3] *Traffic and Granular Flow '99*, edited by D. Helbing, H. J. Herrmann, M. Schreckenberg, and D. E. Wolf (Springer-Verlag, Berlin, 2000).

[4] *Traffic and Granular Flow '01*, edited by M. Fukui, Y. Sugiyama, M. Schreckenberg, and D. E. Wolf (Springer-Verlag, Berlin, 2003).

[5] *Traffic and Granular Flow '03*, edited by S. P. Hoogendoorn, S. Luding, P. H. L. Bovy, M. Schreckenberg, and D. E. Wolf (Springer-Verlag, Berlin, 2005).

[6] *Pedestrian and Evacuation Dynamics*, edited by M. Schreckenberg and S. D. Sharma (Springer-Verlag, Berlin, 2002).

[7] *Pedestrian and Evacuation Dynamics 2003*, edited by E. R. Galea (CMS Press, Greenwich, 2003).

[8] L. F. Henderson, Transp. Res. **8**, 509 (1974).

[9] P. G. Gipps and B. Marksjö, Math. Comput. Simul. **27**, 95 (1985).

[10] D. Helbing and P. Molnar, Phys. Rev. E **51**, 4282 (1995).

[11] D. Helbing, I. J. Farkas, and T. Vicsek, Phys. Rev. Lett. **84**, 1240 (2000).

[12] R. L. Hughes, Math. Comput. Simul. **53**, 367 (2000).

[13] C. Burstedde, K. Klauck, A. Schadschneider, and J. Zittartz, Physica A **295**, 507 (2001).

[14] A. Kirchner and A. Schadschneider, Physica A **312**, 260 (2002).

[15] A. Kirchner, H. Klüpfel, K. Nishinari, A. Schadschneider, and M. Schreckenberg, Physica A **324**, 689 (2003).

[16] A. Kirchner, K. Nishinari, and A. Schadschneider, Phys. Rev. E **67**, 056122 (2003).

[17] A. Nakayama, K. Hasebe, and Y. Sugiyama, Phys. Rev. E **71**, 036121 (2005).

[18] N. Sannomiya and K. Matuda, IEEE Trans. Syst. Man Cybern. **14**, 157 (1984).

[19] C. W. Reynolds, Comput. Graph. (ACM) **21**, 25 (1987).

[20] H. S. Niwa, J. Theor. Biol. **171**, 123 (1994).

[21] T. Vicsek, A. Czirók, E. Ben-Jacob, I. Cohen, and O. Shochet, Phys. Rev. Lett. **75**, 1226 (1995).

[22] H. S. Niwa, J. Theor. Biol. **181**, 47 (1996).

[23] N. Shimoyama, K. Sugawara, T. Mizuguchi, Y. Hayakawa, and M. Sano, Phys. Rev. Lett. **76**, 3870 (1996).

[24] A. Czirók, E. Ben-Jacob, I. Cohen, and T. Vicsek, Phys. Rev. E

54, 1791 (1996).
[25] N. Sannomiya and H. Nakamine, in *Proceedings of the 3rd International Symposium on Artificial Life and Robotics* (AROB, Oita, 1998), Vol. 1, p. 17.
[26] A. Czirok and T. Vicsek, Physica A **281**, 17 (2000).
[27] G. Gregoire and H. Chate, Phys. Rev. Lett. **92**, 025702 (2004).
[28] J. Buhl, D. J. T. Sumpter, I. D. Couzin, J. J. Hale, E. Despland, E. R. Miller, and S. J. Simpson, Science **312**, 1402 (2006).
[29] M. Nagy, I. Daruka, and T. Vicsek, Physica A **373**, 445 (2007).
[30] A. Nakayama and Y. Sugiyama, in *Modeling of Complex Systems: Seventh Granada Lectures*, edited by P. L. Garrido and J. Marro (American Institute of Physics, Melville, NY, 2003), pp. 107–110.
[31] A. Nakayama and Y. Sugiyama, in *Traffic and Granular Flow '03*, edited by S. P. Hoogendoorn, S. Luding, P. H. L. Bovy, M. Schreckenberg, and D. E. Wolf (Springer-Verlag, Berlin, 2005), pp. 399–404.
[32] Y. Sugiyama, A. Nakayama, and E. Yamada, in *Traffic and Granular Flow '05*, edited by A. Schadschneider, T. Poeschel, R. Kuehne, M. Schreckenberg, and D. E. Wolf (Springer-Verlag, Berlin, 2007), pp. 277–282.
[33] By changing interaction terms, some pedestrian models (for example, the social force model) or biological models can be reduced to our model. However, it is difficult to find a relation between those two-dimensional models and one- dimensional model of traffic flow. In contrast, the relation between our model and the one-dimensional OV model is obvious.